# Application of First-Order Feature Analysis of DWI-ADC in Rare Malignant Mesenchymal Tumours of the Maxillofacial Region

**Baoting Yu**
China-Japan Union Hospital of Jilin University
**Chencui Huang**
Beijing Deepwise & League of PHD Technology Co., Ltd
**Shuo Liu**
China-Japan Union Hospital of Jilin University
**Tong Liu**
China-Japan Union Hospital of Jilin University
**Yuyao Guan**
China-Japan Union Hospital of Jilin University
**Xuewei Zheng**
China-Japan Union Hospital of Jilin University
**Jun Ding** ( dingjun_cn@163.com )
China-Japan Union Hospital of Jilin University

**Research**

**Keywords:** Maxillofacial, Mesenchymal tumor, MRI, DWI, Radiomics feature, First order feature

**Posted Date:** January 21st, 2021

**DOI:** https://doi.org/10.21203/rs.3.rs-150873/v1

# Abstract

*Objective:* To research the first-order features of magnetic resonance (MR) diffusion-weighted imaging (DWI)-apparent diffusion coefficient (ADC) in maxillofacial malignant mesenchymal tumours.

*Methods:* Eight patients that the patients' diagnoses were confirmed by pathology, and the clinical and imaging data were determined to be accurate. The patients were all examined by 1.5T MR imaging (MRI). *Results:* PyRadiomics were used to extract radiomics imaging features. The $ADC_{mean}$ and $ADC_{median}$ of sarcoma tissues were 42.2689 and 42.7275, respectively, significantly higher than those in lymphoma tissues ($ADC_{mean}$ (-61.3343) and $ADC_{median}$ (-70.2335)).

*Conclusion:* While the statistical difference is not significant, it is consistent with the outcome of the manual measurement of the ADC mean value of the most significant cross-section of five cases of lymphoma. Development of tumour volume based on the ADC parameter map of DWI demonstrates that the first-order ADC radiomics features analysis can provide new imaging markers for the differentiation of maxillofacial sarcoma and lymphoma. Therefore, first-order ADC features of $ADC_{kurt}$ combined $ADC_{skew}$ may improve the diagnosis level.


# Introduction

The rapid development of MRI in the maxillofacial region has improved the recognition and diagnosis of maxillofacial tumours significantly. The vast majority of malignant maxillofacial tumours originate from epithelial tissue, and mesenchymal tumours are rare. Therefore, the imaging manifestations of these diseases are not well understood, and the rate of clinical misdiagnosis is high. Different types of tumours have different clinical treatment methods. Sarcoma is generally entirely removed by surgery. Chemotherapy is the standard lymphoma treatment. Therefore, it is vital to determine the type of tumour before operating. DWI couled provide essential biomarkers in several kinds of tumours [1, 2].

Radiomics is a new technology whereby algorithms automatically extract and transform a large amount of representative imaging data into exploitable feature spaces that reflect the microscopic characteristics of tumours. [3–4]. MRI could detect and locate the focus and monitor the disease progression that a biopsy cannot.[5, 6]. Recently, radiomics has played an important role in the identification of imaging biomarkers and clinical management.[7–11] However, there are few reports on the application and related literature of maxillofacial mesenchymal tumours. Several rare cases of mesenchymal tumours were analysed retrospectively to provide more reliable clinical evidence for the differential diagnosis of sarcoma and lymphoma. First-order features radiomics analysis[12, 13], as an emerging tool in MRI analysis, could provide insight into tumour heterogeneity and was valuable for differentiating tumour type [14–19] .

In this study, the first-order features of the volume of interests (VOI) were extracted from DWI-ADC parameters. These results, together with the mean ADC were analysed for characterisation of rare malignant mesenchymal tumours in the maxillofacial region.

# 1. Methods

# 1.1 Patients and MRI acquisition parameters

# Patients

Eight patients were retrospectively reviewed (five men, three women; mean age was 51 [range 13–88] years) with a biopsy-proven malignant mesenchymal tumour. The sample patients had preoperative MRI scans between May 2018 and June 2020, and the pathological differentiation could be determined. The sample included three sarcomas and five lymphomas, including one low-grade central osteosarcoma of the left zygoma, two well-differentiated chondrosarcomas of the jaw, one well-differentiated diffuse large B-cell tumour of the buccal region, one B-cell lymphoma related marginal area of tongue mucosa and three non-Hodgkin's follicular lymphoma of the parotid gland. Only patients with sarcomas showed varying degrees of pain and limited facet joint movement, which had no specific clinical symptoms.

The general characteristics of the participants were shown in Table 1. The inclusion criteria: biopsy-proven malignant mesenchymal tumour without concomitant disease. The exclusion criteria were as follows: without definitive post-operative information on pathological characteristics, a minimum tumour diameter < 5 mm, poor MRI quality.

Table 1
The clinical and MRI characteristics of patients (n = 8)

| MR1 scan | Sex | Age | Region | ADC valuc(l0 $^{3}mm^{2}/s$) | Pathological and IHC |
|---|---|---|---|---|---|
| Patient 1 | F | 26 | zygoma | 1.12 | spindie shaped tumor cells and scattered in trabecular bone tissue and bone like matrix tissue; Ki-67( 10–20%), CK(-), SMA and CD99 (+) |
| Patient 2 | F | 40 | jaw | 1.56 | a large number of chondrocytes with obvious heteromorphism and bone septum; viaentin (+), S-100 and CK (-), Ki-67(60%) |
| Patient 3 | M | 56 | jaw | 1.54 | A large number of chondrocytes; S-100(-), Viacntin(+), CK(-), Ki-67(50%) |
| Patient 4 | F | 62 | buccal | 0.56 | Lymphoid hyperplasia; PCK(-), EMA(-), CD20(+), CD79a(+), PAX-5(+), CD3(-), CD38(+), CyclinDI(-), MUMl(-), CD30(-), CD 10(+), Bcl-6(-), Bcl-2(-), CD23(-), CD5(+), Ki67(70%) |
| Patient *5* | M | 88 | tongue | 0.32 | Lymphoid hyperplasia, destroyed lymphoid follicles structure; CD3T(+), BCL-6(-), BCL-2(+), CD 10(-), cyclinDI(-), CD79a(+), Pan-5(+), kappa(-), Ki-67(< 10%) |
| Patient 6 | M | 56 | parotid gland | 0.37 | Lymphoid hyperplasia with obvious heteromorphism; CD3(+), CD20(+), BCL-2(+), BCL-6(+), CD 10(+), Muml(+), PAX-5(+), CD79a(+), Ki-67(70–80%) |
| Patient 7 | M | 67 | parotid gland | 0.54 | Lymphoid hyperplasia, tumor cells infiltrated glands in some areas, serous acini and adipose tissue display; CD20(+), CD 10 (+), CD3 partial cells (+), CD21 showed FDC network, bcl-6 (+), bcl-2 (+), CD38 germinal center positive (+) |
| Patient 8 | M | 13 | parotid gland | 0.57 | -ymphoid hyperplasia, CD3T(+), CD10(-), BCL-6(+), BCL-2(+), CD79a(+), Ki-67(40–50%) |

Table 2
First-order features of sarcomas: $ADC_{kurt}$ $ADC_{skew}$ $ADC_{mean}$ and $ADC_{median}$.

| First-order features | Patient 1 | Patient 2 | Patient 3 | Mean |
|---|---|---|---|---|
| ADCkurt | 3.520680603 | 3.946304522 | 3.280937825 | 3.5826 |
| ADCskew | 0.627515252 | 0.350436023 | 0.391892136 | 0.4566 |
| ADCmean | 180.4899019 | 41.69653962 | -95.37971946 | 42.2689 |
| ADCmedian | 191.38255039999999 | 39.44982554 | -102.6499184 | 42.7275 |

Table 3
First-order features of lymphomas: $ADC_{kurt}$, $ADC_{skew}$, $ADC_{mean}$ and $ADC_{median}$.

| First-order features | Patient 4 | Patient 5 | Patient 6 | Patient 7 | Patient 8 | Mean |
|---|---|---|---|---|---|---|
| **ADCkrut** | 8.259956138 | 6.073467803 | 5.280964199 | 5.827922475 | 4.898098651 | 6.0681 |
| **ADCskew** | 2.142312781 | 1.741374425 | 1.5906607 | 1.302931488 | 1.369502429 | 1.6294 |
| **ADCmean** | -63.95187937 | -34.23833038 | -103.367401 | -39.59149499 | -65.52257619 | -61.3343 |
| **ADCmedian** | -75.86062501 | -48.1006346 | -112.4609443 | -44.98317419 | -69.76222731 | -70.2335 |

# MRI Acquisition Parameters

1.5-T Siemens Avanto with an eight-channel phased-array neck coil was used in this study. The patient's head was secured. Non-contrast axial, sagittal and coronal FS-T2WI sequences acquired in multiple breath-holds were obtained by the following parameters: a repetition/echo time of 5080/87 ms, a slice thickness/interslice gap of 4.0/0.4 mm, 20 slices and a matrix of 256 × 320. Axial T1-weighted images were also acquired in multiple breath-holds. Diffusion-weighted images were obtained in the coronal plane. Following the image acquisition, a pixel-wise ADC map was generated by the inbuilt software using b values of 800 s/mm2. All patients received a 15-ml intravenous bolus injection of gadodiamide (GE Healthcare Ireland Limited, County Cork, Republic of Ireland). The contrast imaging was performed using a fat-suppressed three-dimensional (3D) T1-weighted volumetric interpolated breath-hold examination sequence after the injection.

The shape, size, signal, bone destruction, adjacent tissue relationship on MRI were evaluated. Besides, the ADC map was generated based on DWI, and the sampling was selected to measure the ADC value at the maximum level of the lesion. The lesions were resected surgically in all eight patients. Histopathological and immunohistochemical staining (IHC) was performed postoperatively.

# 1.2 MRI And Radiomics Analysis

Dr Wise Multimodal Research Platform was used for radiomics analysis. An open-source python package called PyRadiomics (2.2.0) was used for extraction of features. The platform supports feature extraction used to calculate single values per feature for an ROI (‘segment-based’) or generate feature maps (‘voxel-based’) (Fig. 1).

# Delineation Of Tumour Roi

The tumour regions in the primary dataset were labeled manually by two experts. In the case of disagreement, a third opinion was requested. The DWI-ADC parameter diagram scan was selected as the labeling image, then tumour tissue was classified.

# Extracting Features From Mri Scans

A B-spline interpolation resampling was used and the anisotropic voxels were resampled to form isotropic voxels of 2.0 mm × 2.0 mm × 2.0 mm. The MRI images were then normalised by centring it at the mean with standard deviation.

$$f(x) = \frac{s(x - \mu_x)}{\sigma x}$$

(s = 100; $\mu_{\square}$ represents mean value; σ represents standard deviation)

Eighteen first-order features were obtained from the original images based on the pixel value extracted from each ROI: Energy, TotalEnergy, MeanAbsolute Deviation, RobustMeanAbsolute Deviation, Entropy, 10Percentile, 90Percentile, Minimum, Maximum, Mean, Median, InterquartileRange, Range, RootMeanSquared, Skewness, Kurtosis, Variance and Uniformity.

# 1.3 Statistical Analysis

The study's group of data obeys the normal distribution and has the homogeneity of variance. SPSS 16.0 (IBM Corp., Armonk, NY, USA) was used. Group differences in quantitative variables were analzed by *t*-test. A *P*-value < 0.05 was considered statistically significant.

## Results

# Imaging and radiomics features

The general characteristics of the eight study participants were listed in Table 1. The sarcomas showed slightly higher signal intensity with b = 800 s/mm$^2$, while ADC images showed a slightly lower signal intensity on DWI images. The average ADC values were 1.12×10$^{-3}$mm$^2$/s□1.56×10$^{-3}$mm$^2$/ s□and 1.54×10$^{-3}$mm$^2$/s. The average of those values is approximately 1.41×10$^{-3}$mm$^2$/s. The average ADC values of lymphomas were lower at 0.56×10$^{-3}$mm$^2$/s□0.31×10$^{-3}$mm$^2$/s□0.37×10$^{-3}$mm$^2$/s□0.54×10$^{-3}$mm$^2$/s□and 0.58×10$^{-3}$mm$^2$/s. The average of those values is approximately 0.47×10$^{-3}$mm$^2$/s.

A total of 18 first-order features were obtained. ADC first-order radiomics feature these parameters: $ADC_{kurt}$ and $ADC_{skew}$ values of sarcomas were 3.5826 and 0.4566 respectively, the values of lymphomas were 6.0681 and 1.6294 respectively (Table 2.3). The $ADC_{kurt}$ and $ADC_{skew}$ differed significantly between sarcoma and lymphoma (P < 0.05), shown in Table 4. The mean values of $ADC_{mean}$ and $ADC_{median}$ of sarcomas were 42.2689 and 42.7275

respectively, which is significantly higher than that of lymphoma ($ADC_{mean}$= -61.3343 and $ADC_{median}$= -70.2335), but the difference was not statistically significant, shown in Table 2.3.

Table 4
Results of the two-sample t-test ($ADC_{kurt}$, $ADC_{skew}$, $ADC_{mean}$ and $ADC_{median}$).

| First-order features | $ADC_{kurt}$ | $ADC_{skew}$ | $ADC_{mean}$ | $ADC_{median}$ |
|---|---|---|---|---|
| P-value | 0.02 | 0.00 | 0.13 | 0.12 |
| (A P-value < 0.05 was considered statistically significant. ) | | | | |

Figure (2-a) shows a low-grade central osteosarcoma of left zygoma with slightly higher ADC value; Fig. (2-b) shows a non-Hodgkin's follicular lymphoma of the right parotid gland with low value. Figure (2-c) shows that lymphoma correlates with an $ADC_{mean}$ in the lower range, positive skew (i.e. high skewness) and a steep curve (i.e. high kurtosis). Sarcoma correlates with a higher $ADC_{mean}$ value, a negative skew (i.e. low skewness), and a flatter shape (i.e. low kurtosis).

# Discussion

In this study, only $ADC_{kurt}$, and $ADC_{skew}$ were significant predictive factors. $ADC_{mean}$ and $ADC_{median}$ were significantly different without statistical significance. The average ADC value of sarcomas is approximately 1.37×10−3mm2/s,and the average ADC value of lymphomas is approximately 0.47×10−3mm2/s. Maeda et al.[20] and Wang et al.[21] found that the average ADC value of lymphoma was lower than head and neck malignant tumours. Furthermore, Sumi et al.[22] reported that an ADC smaller than 0.560×10 − 3 mm2/s could differentiate pharyngeal lymphomas from pharyngeal carcinomas. These results are consistent with our study. Also, the $ADC_{mean}$ (42.2689) and $ADC_{median}$ (42.7275) of sarcoma were significantly higher than the $ADC_{mean}$ (-61.3343) and $ADC_{median}$ (-70.2335) of lymphoma. However, the difference was not statistically significant. These results are consistent with the consequences of manual measurement of the maximum cross-section ADC of five cases of lymphoma. However, the previous study is limited to the review of ADC; there is no distinction between single lymphoma and sarcoma. The cases in this study are rare, which may enrich the clinical data and further improve the understanding of the radiomics features of mesenchymal tumours.

This study found that $ADC_{kurt}$ and $ADC_{skew}$ differed significantly between sarcoma and lymphoma. Lymphoma correlated with an $ADC_{mean}$ in the lower range. Sarcoma correlated with a higher $ADC_{mean}$ value. This study demonstrates that first-order ADC radiomics analysis, used with the average ADC value to improve diagnostic accuracy, could provide new imaging markers for the differentiation of maxillofacial sarcoma and lymphoma. However, more cases need to be studied. Furthermore, there is theoretical support for studying the difference between the first-order characteristics of sarcoma and lymphoma. Besides, Lisson et al. identified several first-order parameters in order to differentiate enchondroma and low-grade osteosarcoma[23]. Meyer et al.[24] reported that texture analysis parameters derived from MRIs could reflect the Ki67 index in soft tissue sarcoma. So, radiomics analysis can reflect microstructure differences between these tumour entities.

DWI had been used in head and neck oncologic imaging. While many researchers focused on the interpretation of conventional CT and MRI, the MRI's imaging extraction feature presents an intriguing way to differentiate sarcoma

and lymphoma.[25–26]. Suo et al.[27] reported that $ADC_{skew}$, $ADC_{kurt}$ and $ADC_{mean}$ differed between benign bladder lesions and bladder carcinoma. Wang et al.[28] applied first-order ADC texture analysis in order to differentiate lymphoma from metastatic nodes in the head and neck region.

DWI could detect non-invasively the diffusion of water molecules in living tissues. The characteristics of the dense distribution of lymphoma cells and small extracellular space can decrease the ADC value.[22] However, cystic degeneration and necrosis are common in sarcomas, and ADC value is slightly higher. Although ADC value is helpful for clinical identification of maxillofacial lymphoma and other diseases, the rate of clinical misdiagnosis is high because of a low incidence rate and typical clinical manifestations. Therefore, more diagnostic criteria are needed, thus increasing the accuracy of clinical diagnosis. Conventional MRI examinations mainly reflect the shape, composition and water molecule diffusion of a tumour. Texture analysis can extract and quantify the grey level, roughness and homogeneity of lesions that cannot be distinguished by the naked eye. That allows the practitioner to reflect on the characteristics of lesions more comprehensively and carefully.[29] Recent studies found that histogram-based parameters reflected the different histopathological features in several tumour entities.[13, 30]. These relationship maybe help to better characterise tumours through radiological imaging and aid in differentiating between tumour types.[31]

Based on the number of cases and features selected in this paper, 18 kinds of first-order features of lesions were extracted for analysis. First-order statistics describe the distribution of voxel intensities. Skewness measures the asymmetry of the distribution of values. A higher kurtosis reflected that distribution mass is concentrated towards the tail(s) rather than towards the mean. Lower kurtosis implies the reverse. Fine texture usually appears in healthy tissue, while rough texture highlights the heterogeneity of the tumour. In this study, the first-order feature analysis of rare cases showed that sarcoma and lymphoma were different in malignant mesenchymal tumours of the maxillofacial region. Therefore, radiomics analysis can provide quantitative parameters in the tumour ROI.

## Limitations

First, the number of patients was limited. Analysing a more significant number of patients' textural parameters may have shown vital information related to tumour characteristics. Second, the differences relating to the imaging parameters and image viewer remains unknown. Future studies of this nature should include a more significant number of cases.

In conclusion, the development of tumour volume based on the ADC parameter map of DWI first-order ADC radiomics analysis makes it possible to provide new imaging markers for the differentiation of maxillofacial sarcoma and lymphoma. Primarily, the feature parameters $ADC_{kurt}$ and $ADC_{skew,}$ combined with the mean ADC value, effectively improves the diagnostic level. However, due to the low incidence rate and a limited number of cases, this study explored only first-order features that were closely related to malignant mesenchymal tumours. It can be concluded from the results of the study that tumour classification can be predicted based on radiomics features, and further study is recommended.

## Abbreviations

MR
magnetic resonance

DWI
diffusion-weighted imaging
ADC
apparent diffusion coefficient
VOI
volume of interests
ROI
region of interest
IHC
immunohistochemical

# Declarations

### Ethics approval and consent to participate

This study was conducted in accordance with the Declaration of Helsinki and approved by the ethics committee of China-Japan Union Hospital of Jilin University.

# Consent for publication

Not applicable.

### Availability of data and materials

All data generated or analyzed during this study are included in this published article

### Competing interests

All of the authors had no any personal, financial, commercial, or academic conflicts of interest separately.


### Funding

Grant support: Health and Health Technology Innovation Project of Jilin Province (2018J078); Discipline Layout Project of Natural Science Foundation of Technology Department of Jilin Province(20200201373JC).


### Authors' contributions

YBT, HCC, LS, LT and GYY conceived of the study, and YBT, ZXW and DJ participated in its design and coordination and YBT helped to draft the manuscript. All authors read and approved the final manuscript.


### Acknowledgements

Not applicable


# References

1. Surov A, Meyer HJ, Wienke A. Correlation between apparent diffusion coefficient (ADC) and cellularity is different in several tumors: a meta-analysis, Oncotarget, vol. 8, no. 35, pp. 59492–59499, 2017.
2. Ravanelli M, Grammatica A, Tononcelli E, Morello R, Leali M, Battocchio S, Agazzi GM, Buglione di Monale E, Bastia M, Maroldi R, Nicolai P, Farina D. Correlation between Human Papillomavirus Status and Quantitative MR Imaging Parameters including Diffusion-Weighted Imaging and Texture Features in Oropharyngeal Carcinoma. AJNR Am J Neuroradiol. 2018;39(10):1878–83.
3. Gillies RJ, Kinahan PE, Hricak H, Radiomics. Images Are More than Pictures, They Are Data, Radiology, vol. 278, no. 2, pp. 563–577, 2016.
4. Lubner MG, Smith AD, Sandrasegaran K, Sahani DV, Pickhardt PJ. CT Texture Analysis: Definitions, Applications, Biologic Correlates, and Challenges, Radiographics, vol. 37, no. 5, pp. 1483–1503, 2017.
5. Soufi M, Arimura H, Nakamoto T, Hirose TA, Ohga S, Umezu Y, Honda H, Sasaki T. Exploration of temporal stability and prognostic power of radiomic features based on electronic portal imaging device images, vol. 46, pp. 32–44, 2018.
6. Li Q, Kim J, Balagurunathan Y, Liu Y, Latifi K, Stringfield O, Garcia A, Moros EG, Dilling TJ, Schabath MB, Ye Z, Gillies RJ. Imaging features from pretreatment CT scans are associated with clinical outcomes in nonsmall-cell lung cancer patients treated with stereotactic body radiotherapy. Med Phys. 2017;44(8):4341–9.
7. Zhou W, Zhang L, Wang K, Chen S, Wang G, Liu Z, Liang C. Malignancy characterization of hepatocellular carcinomas based on texture analysis of contrast-enhanced MR images. J Magn Reson Imaging. 2017;45(5):1476–84.
8. Li Z, Mao Y, Huang W, Li H, Zhu J, Li W, Li B. Texture-based classification of different single liver lesion based on SPAIR T2W MRI images. BMC Med Imaging. 2017;17(1):42.
9. Kim AY, Kim YK, Lee MW, Park MJ, Hwang J, Lee MH, Lee JW. Detection of hepatocellular carcinoma in gadoxetic acid-enhanced MRI and diffusion-weighted MRI with respect to the severity of liver cirrhosis. Acta Radiol. 2012;53(8):830–8.
10. Makanyanga J, Ganeshan B, Rodriguez-Justo M, Bhatnagar G, Groves A, Halligan S, Miles K, Taylor SA. MRI texture analysis (MRTA) of T2-weighted images in Crohn's disease may provide information on histological and MRI disease activity in patients undergoing ileal resection. Eur Radiol. 2017;27(2):589–97.
11. Li M, Fu S, Zhu Y, Liu Z, Chen S, Lu L, Liang C. Computed tomography texture analysis to facilitate therapeutic decision making in hepatocellular carcinoma. Oncotarget, vol. 7, no. 11, pp. 13248–13259, 2016.
12. Davnall F, Yip CS, Ljungqvist G, Selmi M, Ng F, Sanghera B, Ganeshan B, Miles KA, Cook GJ, Goh V. Assessment of tumor heterogeneity: an emerging imaging tool for clinical practice? Insights Imaging, vol. 3, no. 6, pp. 573–589, 2012.
13. Just N. Improving tumour heterogeneity MRI assessment with histograms. Br J Cancer. 2014;111(12):2205–13.
14. Downey K, Riches SF, Morgan VA, Giles SL, Attygalle AD, Ind TE, Barton DP, Shepherd JH, deSouza NM. Relationship between imaging biomarkers of stage I cervical cancer and poor-prognosis histologic features: quantitative histogram analysis of diffusion-weighted MR images. AJR Am J Roentgenol. 2013;200(2):314–20.
15. Woo S, Cho JY, Kim SY, Kim SH. Histogram analysis of apparent diffusion coefficient map of diffusion-weighted MRI in endometrial cancer: a preliminary correlation study with histological grade. Acta Radiol. 2014;55(10):1270–7.

16. Takahashi M, Kozawa E, Tanisaka M, Hasegawa K, Yasuda M, Sakai F. Utility of histogram analysis of apparent diffusion coefficient maps obtained using 3.0T MRI for distinguishing uterine carcinosarcoma from endometrial carcinoma. J Magn Reson Imaging. 2016;43(6):1301–7.
17. Hao Y, Pan C, Chen W, Li T, Zhu W, Qi J. Differentiation between malignant and benign thyroid nodules and stratification of papillary thyroid cancer with aggressive histological features: Whole-lesion diffusion-weighted imaging histogram analysis. J Magn Reson Imaging. 2016;44(6):1546–55.
18. Liang H-Y, Huang Y-Q, Yang Z-X, Ying-Ding, Zeng M-S, Rao S-X. Potential of MR histogram analyses for prediction of response to chemotherapy in patients with colorectal hepatic metastases. Eur Radiol. 2016;26(7):2009–18.
19. Kyriazi S, Collins DJ, Messiou C, Pennert K, Davidson RL, Giles SL, Kaye SB, Desouza NM. Metastatic ovarian and primary peritoneal cancer: assessing chemotherapy response with diffusion-weighted MR imaging–value of histogram analysis of apparent diffusion coefficients, Radiology, vol. 261, no. 1, pp. 182–192, 2011.
20. Maeda M, Kato H, Sakuma H, Maier SE, Takeda K. Usefulness of the apparent diffusion coefficient in line scan diffusion-weighted imaging for distinguishing between squamous cell carcinomas and malignant lymphomas of the head and neck. AJNR Am J Neuroradiol. 2005;26(5):1186–92.
21. Wang J, Takashima S, Takayama F, Kawakami S, Saito A, Matsushita T, Momose M, Ishiyama T. Head and neck lesions: characterization with diffusion-weighted echo-planar MR imaging, Radiology, vol. 220, no. 3, pp. 621–630, 2001.
22. Sumi M, Ichikawa Y, Nakamura T. Diagnostic ability of apparent diffusion coefficients for lymphomas and carcinomas in the pharynx. Eur Radiol. 2007;17(10):2631–7.
23. Lisson CS, Lisson CG, Flosdorf K, Mayer-Steinacker R, Schultheiss M, von Baer A, Barth TFE, Beer AJ, Baumhauer M, Meier R, Beer M, Schmidt SA. Diagnostic value of MRI-based 3D texture analysis for tissue characterisation and discrimination of low-grade chondrosarcoma from enchondroma: a pilot study. Eur Radiol. 2018;28(2):468–77.
24. Meyer HJ, Renatus K, Höhn AK, Hamerla G, Schopow N, Fakler J, Josten C, Surov A. Texture analysis parameters derived from T1-and T2-weighted magnetic resonance images can reflect Ki67 index in soft tissue sarcoma, Surg Oncol, vol. 30, pp. 92–97, 2019.
25. Kierans AS, Doshi AM, Dunst D, Popiolek D, Blank SV, Rosenkrantz AB. Retrospective Assessment of Histogram-Based Diffusion Metrics for Differentiating Benign and Malignant Endometrial Lesions. J Comput Assist Tomogr. 2016;40(5):723–9.
26. Suo S, Zhang K, Cao M, Suo X, Hua J, Geng X, Chen J, Zhuang Z, Ji X, Lu Q, Wang H, Xu J. Characterization of breast masses as benign or malignant at 3.0T MRI with whole-lesion histogram analysis of the apparent diffusion coefficient. J Magn Reson Imaging. 2016;43(4):894–902.
27. Suo ST, Chen XX, Fan Y, Wu LM, Yao QY, Cao MQ, Liu Q, Xu JR. Histogram analysis of apparent diffusion coefficient at 3.0 T in urinary bladder lesions: correlation with pathologic findings, Acad Radiol, vol. 21, no. 8, pp. 1027–1034, 2014.
28. Wang YJ, Xu XQ, Hu H, Su GY, Shen J, Shi HB, Wu FY. Histogram analysis of apparent diffusion coefficient maps for the differentiation between lymphoma and metastatic lymph nodes of squamous cell carcinoma in head and neck region, Acta Radiol, vol. 59, no. 6, pp. 672–680, 2018.
29. Lambin P, Leijenaar RTH, Deist TM, Peerlings J, de Jong EEC, van Timmeren J, Sanduleanu S, Larue RTHM, Even AJG, Jochems A, van Wijk Y, Woodruff H, van Soest J, Lustberg T, Roelofs E, van Elmpt W, Dekker A,

Mottaghy FM, Wildberger JE, Walsh S. Radiomics: the bridge between medical imaging and personalized medicine. Nat Rev Clin Oncol. 2017;14(12):749–62.

30. Schob S, Meyer HJ, Pazaitis N, Schramm D, Bremicker K, Exner M, Höhn AK, Garnov N, Surov A. ADC Histogram Analysis of Cervical Cancer Aids Detecting Lymphatic Metastases-a Preliminary Study. Mol Imaging Biol. 2017;19(6):953–62.
31. Liu S, Zhang Y, Chen L, Guan W, Guan Y, Ge Y, He J, Zhou Z. Whole-lesion apparent diffusion coefficient histogram analysis: significance in T and N staging of gastric cancers. BMC Cancer. 2017;17(7):665.

# Figures

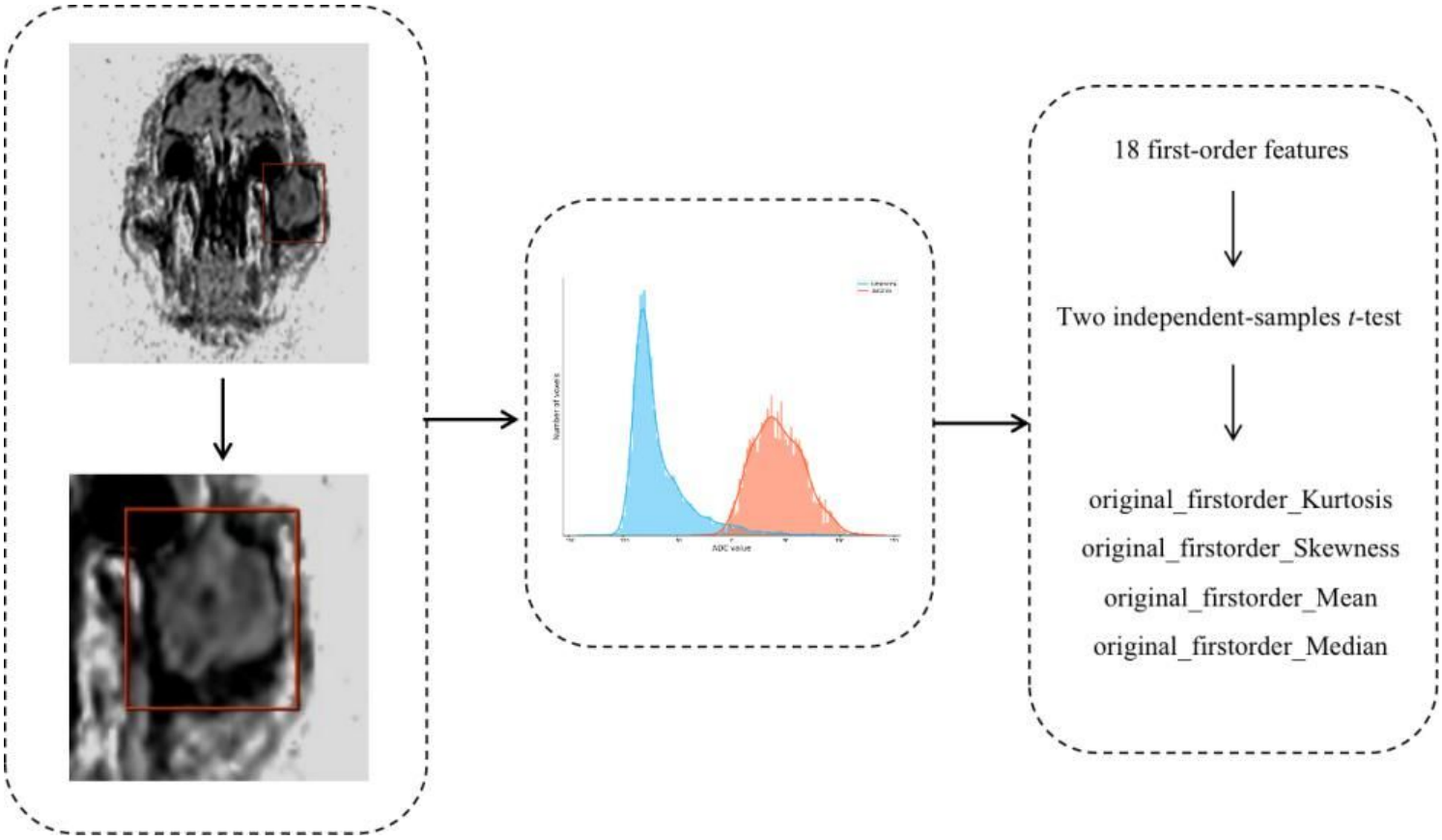


**Figure 1**

First-order ADC radiomics analysis scheme used in this study.

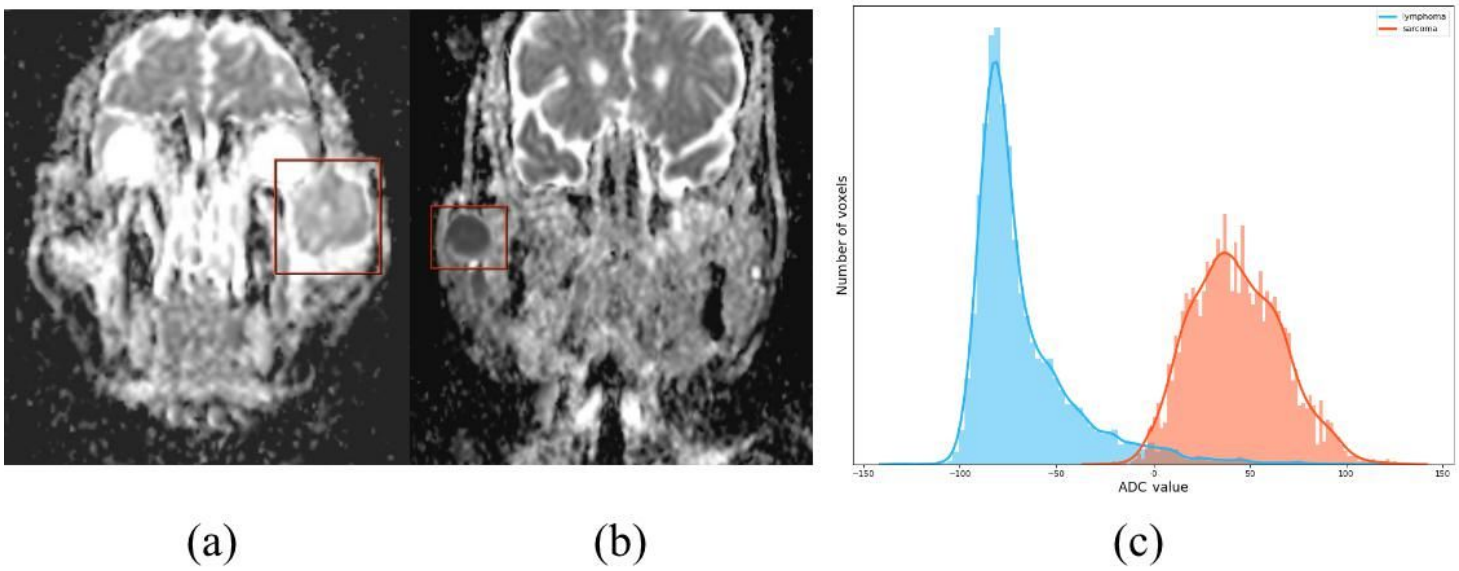


## Figure 2

DWI-ADC images of (a) scarcoma and (b) lymphoma. (a) A 28 years old female patient with a sarcoma within the left zygoma, DWI-ADC image the lesion appears relatively inhomogeneous slightly higher signal compared to the adjacent muscle. ADC value is about 1.12 mm2/s; (b) A 67 years old male patient with a lymphoma within the right parotid gland, DWI-ADC image the lesion appears relatively homogeneous lower signal compared to the adjacent muscle. ADC value is about 0.54 mm2/s; (c) Lymphoma correlating with an ADCmean in the lower range, positive skew (high skewness), and a steep curve (high kurtosis). Sarcoma correlating with a higher ADCmean value, a negative skew (low skewness), and a flatter shape (low kurtosis).